Mon. Not. R. Astron. Soc. **000**, 000–000 (0000) Printed 2 February 2008 (MN LATEX style file v2.2)

The role of AGN in the colour transformation of galaxies at redshifts $z \approx 1$

A. Georgakakis[1⋆], K. Nandra[1], R. Yan[2], S. P. Willner[3], J. M. Lotz[4,5], C. M. Pierce[4], M. C. Cooper[2,6], E. S. Laird[1], D. C. Koo[7], P. Barmby[3], J. A. Newman[8], J. R. Primack[9] A. L. Coil[6]

[1]*Astrophysics Group, Blackett Laboratory, Imperial College, Prince Consort Rd , London SW7 2BZ, UK*
[2]*Department of Astronomy, University of California, Berkeley, CA 94720*
[3]*Harvard-Smithsonian Center for Astrophysics, 60 Garden Street, MailStop 65, Cambridge, MA02138, USA*
[4]*Department of Physics, University of California, Santa Cruz, 1156 High Street, CA 95064, USA*
[5]*National Optical Astronomical Observatories, 950 N. Cherry Avenue, Tucson, AZ 85719, USA*
[6]*Steward Observatory, University of Arizona, 933 N. Cherry Ave., Tucson, AZ 85721-0065, USA*
[7]*UCO/Lick Observatory and Department of Astronomy & Astrophysics, University of California, Santa Cruz, CA 95064, USA*
[8]*Lawrence Berkeley National Laboratory, Berkeley, CA 94720, USA*
[9]*Department of Physics, University of California, Santa Cruz, 1156 High St., Santa Cruz, CA 95064, USA*

2 February 2008

ABSTRACT

We explore the role of AGN in establishing and/or maintaining the bimodal colour distribution of galaxies by quenching their star-formation and hence, causing their transition from the blue to the red cloud. Important tests for this scenario include (i) the X-ray properties of galaxies in the transition zone between the two clouds and (ii) the incidence of AGN in post-starbursts, i.e. systems observed shortly after (< 1 Gyr) the termination of their star-formation. We perform these tests by combining deep *Chandra* observations with multiwavelength data from the AEGIS survey. Stacking the X-ray photons at the positions of galaxies ($0.4 < z < 0.9$) not individually detected at X-ray wavelengths suggests a population of obscured AGN among sources in the transition zone and in the red cloud. Their mean X-ray and mid-IR properties are consistent with moderately obscured low-luminosity AGN, Compton thick sources or a mix of both. Morphologies show that major mergers are unlikely to drive the evolution of this population but minor interactions may play a role. The incidence of obscured AGN in the red cloud (both direct detections and stacking results) suggests that BH accretion outlives the termination of the star-formation. This is also supported by our finding that post-starburst galaxies at $z \approx 0.8$ and AGN are associated, in agreement with recent results at low-z. A large fraction of post-starbursts and red cloud galaxies show evidence for at least moderate levels of AGN obscuration. This implies that if AGN outflows cause the colour transformation of galaxies, then some nuclear gas and dust clouds either remain unaffected or relax to the central galaxy regions after quenching their star-formation.

Key words: Surveys – galaxies: active – galaxies: bulges – galaxies: evolution – galaxies: interactions – cosmology: observations

1 INTRODUCTION

A major recent development in extragalactic astronomy is the discovery that most of the spheroids in the local Universe contain a super-massive black hole (BH; e.g. Magorrian et al. 1998). The masses of these monsters are tightly correlated to the stellar velocity dispersion of the host galaxy bulges (e.g. Ferrarese et al. 2000; Gebhardt et al. 2000), suggesting that the formation and evolution of spheroids and the build-up of the super-massive BHs at their centres are interconnected. This interplay may hold the key for understanding some of the observed trends in galaxy evolution.

One of the fundamental properties of galaxies is their bimodal

⋆ Marie Curie fellow

distribution in rest-frame colour. This bimodality is observed to beyond redshift $z \approx 1$ and is believed to hold important clues on galaxy assembly (e.g. Strateva et al. 2001; Baldry et al. 2004; Bell et al. 2004; Weiner et al. 2005; Cirasuolo et al. 2007). Evolved spheroidal galaxies are found in the "red-cloud" of the colour-magnitude diagram (CMD), star-forming systems define the "blue cloud", while the region between these overdensities is sparsely populated. This bimodal distribution is likely to be the combined result of evolution effects and external factors such as interactions and mergers (e.g. Bell et al. 2004, 2006a, 2006b; Blanton 2006). In the simplest interpretation, the CMD is consistent with a picture where the galaxy star-formation is truncated, by a mechanism that remains to be identified, leading to the ageing of the stellar population and the rapid transition from the blue to the red cloud. AGN are proposed to play a major part in this process by regulating the star-formation in galaxies causing their transition in colour or maintaining them in the red cloud.

Modelling work indeed suggests that the energy released by AGN is sufficient to either heat up or blow away the cold gas of galaxies (e.g. Silk & Rees 1998; Fabian 1999; King 2003), irreversibly altering their evolution. Two main routes are proposed by which AGN feedback affects the host galaxy. The first one operates during the luminous and high accretion rate stage of BH growth, which is suggested to occur during major mergers (Hopkins et al. 2005, 2006a, b). These catastrophic events also produce nuclear starbursts that obscure the central engine for most of its active lifetime. When the AGN becomes sufficiently luminous it drives outflows, which sweep away the nuclear gas and dust clouds, thereby quenching the nuclear star-formation. Following this stage, the AGN also declines as the BH runs out of accreting material and eventually switches off.

In addition to the cold gas accretion mode above, simulations also include a second AGN feedback recipe, which is invoked to suppress the accretion of hot gas onto the central galaxy of large dark matter haloes (e.g. Croton et al. 2006; Okamoto et al. 2007; Cattaneo et al. 2007). This mode operates in systems where the supermassive BHs have already been built through mergers and are in place at the central galaxy regions. In this picture, as galaxies enter the massive dark matter haloes of groups or clusters, their cold gas supply is cut off leading to passive evolution and their migration to the red cloud (Dekel & Birnboim 2006; Croton et al. 2006). However, cooling flows in these dense environments could produce a reservoir of cold gas in the central galaxy regions, the raw material for starburst and QSO activity. Low-level BH accretion is therefore invoked to counterbalance cooling flows by producing low-luminosity AGN that heat the bulk of the cooling gas and thereby suppressing any subsequent star-formation in these galaxies.

In the two AGN feedback prescriptions above, the outflow scenario during the luminous and high accretion rate phase of BH growth, assigns AGN a central role in establishing the bimodal colour distribution of galaxies by directly causing their transition from the blue to the red cloud. The distribution of X-ray selected AGN in the CMD appears to be broadly consistent with this picture. AGN are preferentially associated with galaxies in the red cloud, at the red limit of the blue cloud and in the transition zone in between. These associations are suggestive of AGN-driven truncation of the star-formation (Nandra et al. 2007). However, more detailed study of the properties of AGN reveal a number of inconsistencies with the merger scenario. Obscured AGN are predominantly hosted by galaxies in the red cloud (Nandra et al. 2007; Rovilos & Georgantopoulos 2007), with prominent bulges and little morphological evidence for ongoing major mergers (Grogin et al. 2003; Pierce et al. 2007). The red optical colours of these systems are most likely because of old stars and not dusty star-formation. Although there are examples of deeply buried AGN in star-forming galaxies (e.g. Genzel et al. 1998; Cid Fernandes et al. 2001; Franceschini et al. 2003; Georgakakis et al. 2004; Alexander et al. 2005), the frequency of these systems among the obscured X-ray population at $z \approx 1$ is not yet clear. For example, Rovilos et al. (2007) argue that a non-negligible fraction of X-ray selected AGN at $z \approx 1$ have μJy radio continuum emission (1.4 GHz) that is consistent with star-formation in the host galaxy. These authors however, do not find a strong trend between X-ray obscuration and the incidence of faint radio emission, likely to be associated with starbursts.

A plausible interpretation of the evidence above is that current X-ray surveys are biased against the early phase of BH evolution. At this initial stage of their formation, AGN may be deeply buried under star-forming clouds and/or low luminosity because the BH mass is still small, although growing rapidly. If there is such a population of obscured and/or intrinsically faint young AGN below the detection threshold of current surveys, it may be possible to find them using stacking analysis. Alternatively, AGN may not be responsible for quenching the star-formation in galaxies and producing the bimodality of the CMD. A key test of this scenario is the incidence of AGN in post-starburst galaxies, i.e. systems observed shortly after the termination of their star-formation (< 1 Gyr). In the local Universe ($z \lesssim 0.1$), a number of studies point to an association between *optically* selected AGN and post-starbursts (e.g. Kauffmann et al. 2004; Goto 2006; Yan et al. 2006). At $z \approx 1$, close to the peak of the AGN density in the Universe (e.g. Barger et al. 2005; Hasinger et al. 2005), there is still very limited information on the link between X-ray selected AGN and post-starbursts.

We address the issues above using data from the All-wavelength Extended Groth strip International Survey (AEGIS; Davis et al. 2007). X-ray stacking is employed to search for deeply buried and/or low-luminosity AGN among optically selected galaxies in the redshift interval $0.4 < z < 0.9$ to explore the role of BH accretion in establishing the bimodal colour distribution of these systems. We also study the X-ray properties of post-starbursts as identified from Keck spectra at $z \approx 0.8$ to investigate the link between recent star-formation events and active BHs. We adopt $\mathrm{H}_0 = 70\,\mathrm{km\,s^{-1}\,Mpc^{-1}}$, $\Omega_\mathrm{M} = 0.3$ and $\Omega_\Lambda = 0.7$.

2 MULTIWAVELENGTH OBSERVATIONS

Details about the AEGIS datasets can be found in Davis et al. (2007). In this paper we use (i) the deep *Chandra* observations to explore the X-ray properties of optical galaxies with spectroscopic redshifts from the DEEP2 survey, (ii) the *Spitzer* IRAC and MIPS $24\,\mu$m data to select subsamples based on mid-IR colour, and (iii) the high resolution *HST*/ACS imaging for morphological studies.

The X-ray data are from the *Chandra* survey of the Extended Groth Strip (EGS). The observations consist of 8 ACIS-I pointings, each with a total integration time of about 200 ks split in at least 3 shorter exposures obtained at different epochs. The data reduction, source detection and flux estimation are described in detail by Nandra et al. (2007, in preparation) and are based on methods presented by Nandra et al. (2005). Briefly, standard reduction steps are taken using the CIAO version 3.2 data analysis software. After merging the individual observations into a single event file, we constructed images in four energy bands 0.5-7.0 keV (full), 0.5-2.0 keV (soft), 2.0-7.0 keV (hard) and 4.0-7.0 keV (ultra-hard). The count rates in the above energy intervals are converted to fluxes in the

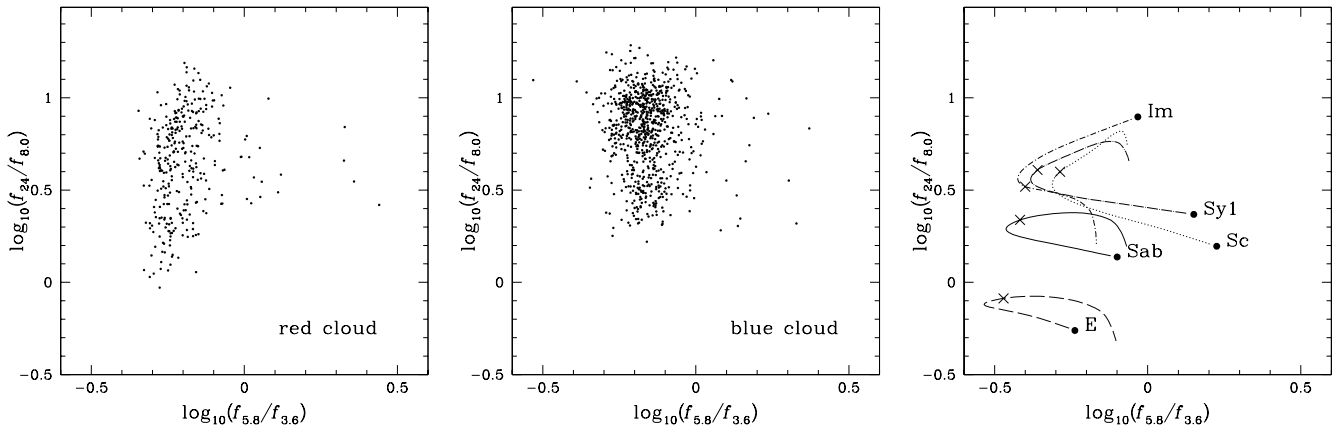

Figure 2. Mid-IR colour-colour plot. For clarity we use different panels. Left: red cloud galaxies in the redshift range $0.4-0.9$. Middle: blue cloud galaxies in the same redshift interval. In both panels we only plot sources detected in all 4 IRAC/MIPS bands used to estimate colours. Right: expected tracks of different galaxy types in the range $z = 0-1$ using observed mid-IR SEDs from the SINGS described by Dale et al. (2007). NGC 1097 Sy1: long-dashed dotted; NGC 5408 Im: short-dashed dotted; Sc spiral galaxy NGC 628: dotted; Sab spiral NGC 4450: continuous; elliptical galaxy NGC 584: long dashed. The dots mark the position of $z = 0$ and the crosses correspond to $z = 0.4$.

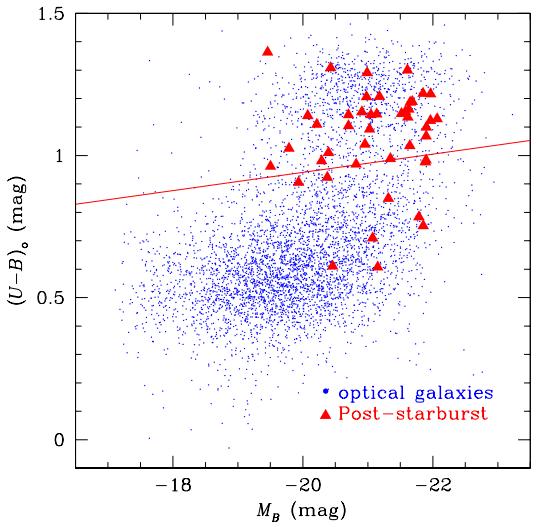

Figure 1. Rest-frame $U-B$ colour against B-band absolute magnitude for DEEP2 galaxies (small blue dots) in the range $0.4 < z < 0.9$ estimated by Willmer et al. (2006). Post-starburst galaxies are shown with the (red) triangles. The continuous line is defined by Willmer et al. (2006) to separate the red from the blue clouds.

standard bands 0.5-10, 0.5-2, 2-10 and 5-10 keV, respectively. The limiting flux in each of these bands is estimated to be 3.5×10^{-16}, 1.1×10^{-16}, 8.2×10^{-16}, and 1.4×10^{-15} erg s^{-1} cm^{-2}, respectively. The X-ray catalogue comprises a total of 1318 sources over $0.63\,\mathrm{deg}^2$ to a Poisson detection probability threshold of 4×10^{-6}. At $z \approx 1$ the 2-10 keV limit above corresponds to an X-ray luminosity of about 3×10^{42} erg s^{-1} ($\Gamma = 1.4$), i.e. typical of Seyferts. For the optical identification we use the DEEP2 photometric catalogues and the Likelihood Ratio (LR) method (e.g. Brusa et al. 2007). A total of 903 sources have counterparts to $R_{AB} = 25$ mag ($LR > 0.7$), the approximate limit of the DEEP2 photometric survey.

The DEEP2 redshift survey uses the DEIMOS spectrograph (Faber et al. 2003) on the 10 m Keck-II telescope to obtain redshifts for galaxies to $R_{AB} = 24.1$ mag. The observational setup uses a moderately high resolution grating ($R \approx 5000$), which provides a velocity accuracy of $30\,\mathrm{km\,s^{-1}}$ and a wavelength coverage of 6500–9100 Å. This spectral window allows the identification of the strong [O II] doublet 3727Å emission line to $z < 1.4$. We use DEEP2 galaxies with redshift determinations secure at the $> 90\%$ confidence level (quality flag $Q \geqslant 3$; Davis et al. 2007).

The *Spitzer* IRAC and MIPS-24μm observations cover the central $10 \times 120\,\mathrm{arcmin}^2$ subregion of the EGS (Barmby et al. 2006). The integration time is about 2.7 hr and 1200 s per pointing for the IRAC and MIPS observations, respectively. The 5σ flux density limit for point sources is 0.9, 5.8 and 83 μJy at 3.6, 8.0 and 24 μm, respectively. There are about 57 400, 13 600 and 6 300 detections to the limits above. These sources are matched to the DEEP2 photometric catalogue by finding the nearest neighbour within a search radius of 1.0 arcsec.

HST images of the EGS were taken with the Advanced Camera for Surveys (ACS) in the V (F606W, 2260s) and I (F814W, 2100s) filters over a $10.1 \times 70.5\,\mathrm{arcmin}^2$ strip (Lotz et al. 2007). The 5 sigma limiting magnitudes for a point source are $V_{F606W} = 28.14$ (AB) and $I_{F814W} = 27.52$ (AB). For extended sources these limits are about 2 mag brighter. A total of 15 797 galaxies were detected to $I_{F814W} = 25$ mag. These were matched to the DEEP2 photometric catalogue using an 1.0 arcsec matching radius.

3 SAMPLE SELECTION

The main sample used in this paper consists of optically selected galaxies with DEEP2 spectroscopy and redshifts in the interval $0.4 < z < 0.9$. This redshift range is to minimise colour dependent biases in the selection of galaxies introduced by the magnitude limit of the DEEP2 spectroscopic survey, $R_{AB} < 24.1$ mag. Red cloud sources drop below the survey limit at lower redshifts than intrinsically bluer galaxies (e.g. Gerke et al. 2007). This effect becomes increasingly severe at $z \gtrsim 1$ as the R-band straddles the rest-frame UV. At $z = 0.9$ the sample is complete to $M_B = -20$ mag. The

lower redshift cut, $z = 0.4$, is to avoid biases associated with the small volume sampled by the AEGIS below this limit.

There are 4814 sources in the main galaxy sample of which about 70 per cent overlap with the *Spitzer* IRAC and MIPS surveys of the AEGIS and 30 per cent have I-band morphological information from the HST/ACS observations. The morphological sample was compiled using the criteria of Lotz et al. (2007) by selecting galaxies brighter than $I_{F814W} = 25$ mag with average signal-to-noise ratio per pixel >2.5 and petrosian radius > 0.3 arcsec. About 65 per cent of the sources detected on the HST/ACS images fulfil these criteria. Almost all of them (97 per cent) overlap with the IRAC/MIPS area.

The CMD of the main galaxy sample is presented in Figure 1. The blue and red clouds are defined using the relation of Willmer et al. (2006). Galaxies with $U - B$ colours ± 0.05 about this relation define the valley between the two clouds. Willmer et al. (2006) find that the redshift evolution of the red galaxy population $U - B$ colour is not strong in DEEP2. As a result a line with fixed normalisation is adequate for defining the blue and red clouds over the redshift interval of our sample. The next sections discuss the properties of galaxies in narrow slices of the CMD. These are defined to run parallel to the Willmer et al. (2006) line separating the two clouds and are parametrised by their distance in $U-B$ colour, ΔC, from that line.

The post-starburst sub-sample was drawn from the main galaxy sample following the method described by Yan et al. (2006, 2007 in prep.). The continuum-subtracted DEEP2 optical spectra were fit with a combination of an old (K-component) and a young (A-component) stellar population SED. Post-starburst candidates are defined as systems with $f_A > 0.25$, where f_A is the fraction of light contributed by the young stellar component around 4500Å in the linear decomposition of the spectrum. The equivalent width of Hβ, after the removal of the stellar absorption, was then used to identify residual/ongoing star-formation activity within the sample. Yan et al. (2006) showed that, for high redshift galaxies, this line is a more reliable star-formation indicator than the [OII] 3727 line, which is often associated with AGN activity. Post-starbursts (K+As) are defined as systems with little Hβ emission, $\mathrm{EW(H}\beta) < 5\, f_A - 1$ (total of 44). Because of the wavelength coverage of the DEEP2 spectroscopy, post-starbursts can be identified only in the redshift slice $0.68 - 0.88$. In this interval, the DEEP2 spectral window includes the Hβ line as well as the rest-frame wavelength range $3900 \lesssim \lambda \lesssim 4900$Å, which is essential for the decomposition of the spectrum into an old and a young stellar components. Figure 1 shows the position of post-starbursts in the CMD. Most of them are in the red cloud.

The mid-IR SED of galaxies results from a combination of cirrus radiation, stellar emission, dusty star-formation, and possibly hot dust associated with an AGN. Samples selected at $24\,\mu$m are generally dominated by dust enshrouded galaxies, both AGN and starbursts (e.g. Yan et al. 2004). In this paper, we will use the $24\,\mu$m emission to identify such systems and to study them separately from quiescent galaxies. Figure 2 presents the *Spitzer* IRAC/MIPS colours of DEEP2/AEGIS sources. Also shown in this plot are the colour tracks for different galaxy types using a selection of observed SEDs from the SINGS program (Dale et al. 2007). Undoubtedly there are large intrinsic variations in the mid-IR properties of galaxies of a given type resulting in a range of mid-IR colours. Nevertheless, the general trend in Figure 2 is for quiescent systems to occupy the lower part of the plot and star-formation or AGN activity to produce redder mid-IR colours. In this paper we define "$24\,\mu$m–bright" sources as those with $\log(f_{24}/f_{8.0}) > 0.4$. Bluer mid-IR colours ($\log(f_{24}/f_{8.0}) < 0.4$) or no detection at $24\,\mu$m defines the "$24\,\mu$m–faint" sample. The latter sample is likely to include "$24\,\mu$m–bright" sources that are below the detection limit of the $24\,\mu$m observations. As expected most of the $24\,\mu$m selected sources lie above the $\log(f_{24}/f_{8.0}) > 0.4$ cut in Figure 2. Quiescent galaxies are nevertheless also present in that sample.

Table 1. Fraction of X-ray detections in different subsamples

Sample	N_{TOT}	N_X	f_X (%)
(1)	(2)	(3)	(4)
red $0.4 < z < 0.7$	548	36	6.5 ± 1.1
red $0.7 < z < 0.9$	490	20	4.1 ± 1.0
red post-starburst	34	5	14.7 ± 7.0
valley $0.4 < z < 0.7$	105	4	3.8 ± 1.9
valley $0.7 < z < 0.9$	126	8	6.3 ± 2.3
valley post-starburst	9	1	11 ± 11
blue $0.4 < z < 0.7$	2007	24	1.2 ± 0.2
blue $0.7 < z < 0.9$	1769	28	1.5 ± 0.3
blue post-starburst	10	2	20 ± 15

The columns are: (1): Sample definition. Note that there is overlap between the red or the blue cloud and the valley. The redshift interval $0.7 < z < 0.9$ is comparable in terms of selection effects to post-starburst galaxies; (2): N_{TOT} is the total number of DEEP2 galaxies in the sample; (3): N_X corresponds to the number of DEEP2 galaxies with X-ray counterparts; (4): f_X is the fraction of X-ray detections in the sample, i.e. $f_X = N_X/N_{TOT}$. The errors are estimated assuming Poisson statistics.

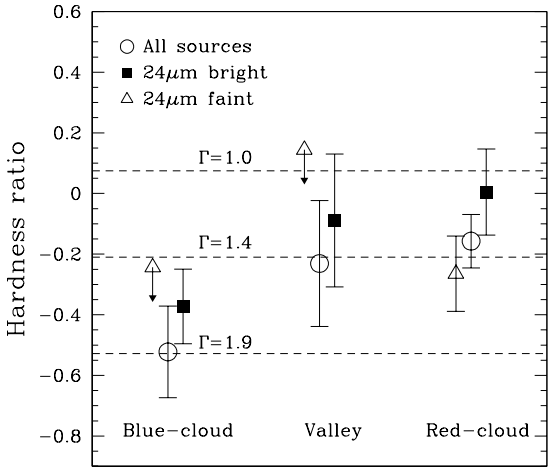

Figure 3. Mean hardness ratio for galaxies in the blue/red clouds and the valley. Within each of these 3 groups, open circles correspond to all sources in the group, squares are for $24\,\mu$m bright galaxies, and triangles represent $24\,\mu$m faint systems. The hardness ratio uncertainties are estimated assuming Poisson statistics. In the case of no detection in the hard band, the 3σ upper limit in the hardness ratio is plotted. The horizontal lines correspond to the expected hardness ratio of a power-law X-ray spectrum with spectral index from top to bottom $\Gamma = 1.0$, 1.4 and 1.9, respectively. Despite the error bars, there is evidence for hardening of the mean X-ray spectrum from the blue to the red cloud. $24\,\mu$m bright sources have harder spectra in each group.

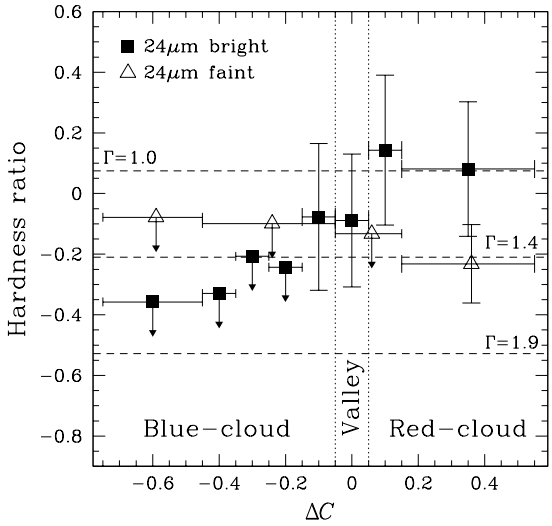

Figure 4. Mean hardness ratio estimated by stacking optical galaxies within different slices of the CMD. ΔC is defined as the difference between the colour of the galaxy and the line separating the blue from the red clouds (Willmer et al. 2006; see Fig. 1). The colour slices are parallel to this line and their position in the CMD depends on M_B. The vertical dotted lines define the valley between the red and the blue clouds. The horizontal dashed lines are the same as in Figure 3. The line of $\Gamma = 1.4$ corresponds to the mean hardness ratio of the X-ray detected AGN. 24 μm-bright and 24 μm-faint systems are shown with the squares and the triangles respectively. The horizontal error bar of each point corresponds to the width of the CMD slice within which galaxies are stacked. The hardness ratio uncertainties are estimated assuming Poisson statistics. In the case of no detection in the hard band, the 3σ upper limit in the hardness ratio is plotted (arrows pointing downward).

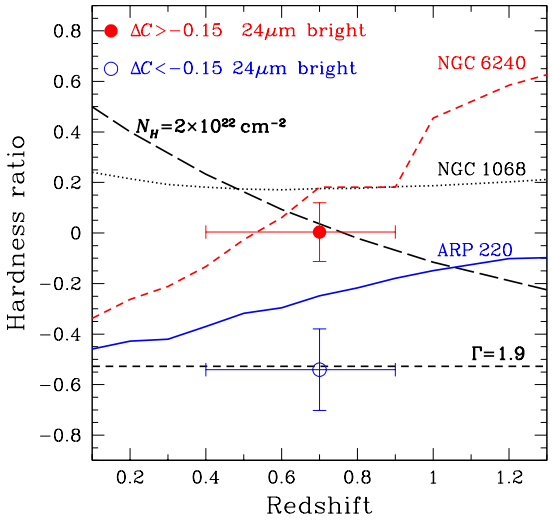

Figure 5. Hardness ratio against redshift. The curves are the expected tracks for the ARP 220 dusty starburst (Ptak et al. 2003), the Compton thick AGN NGC 1068 (Matt et al. 1999) and NGC 6240 (Ptak et al. 2003) and a simple absorbed power-law model with $\Gamma = 1.9$ and $N_H = 2 \times 10^{22}\,\mathrm{cm}^{-2}$. The short-dashed line corresponds to power-law X-ray spectrum with $\Gamma = 1.9$, typical of unabsorbed AGN. The filled (red) circle corresponds to red 24μm-bright galaxies with $\Delta C > -0.15$. The open (blue) circle is for blue 24μm-bright galaxies with $\Delta C < -0.15$.

4 THE X-RAY STACKING METHOD

The mean X-ray properties of sources which are not individually detected to the limit of the X-ray survey are explored using stacking analysis (e.g. Nandra et al. 2002; Laird et al. 2005). We used a fixed radius aperture to extract and to sum the X-ray photons at the positions of optically selected galaxies. Sources that are separated from an X-ray detection by less than 1.5 times the local 90 per cent Encircled Energy Fraction (EEF) radius are excluded from the stacking. This is to avoid contamination of the stacked signal from photons associated with the Point Spread Function (PSF) wings of X-ray detections. Also, in order to exclude regions where the *Chandra* PSF is large and the sensitivity is low, we do not extract photons from pointings where a particular source is located more than 9 arcmin away from the centre of the detector. This off-axis angle cutoff is chosen to maximise the stacked signal, although our results are not particularly sensitive to this parameter. For the extraction radius, we experimented with apertures in the range 1–3 arcsec and selected 2 arcsec as the optimal radius that maximises the signal-to-noise ratio of the stacked X-ray photons.

To assess the significance of the stacked signal, we estimated the local background of a particular source by averaging the X-ray photons within a 50 arcsec radius (100 pixels) and then scaling to the area of the extraction aperture. When determining the local background we clipped regions around X-ray detections using a radius 1.5 times larger than the 90 per cent EEF. The significance (in sigma) of the stacked signal is estimated by $(T - B)/\sqrt{B}$, where T and B are the total (source + background) and background counts respectively. The 2 arcsec radius includes only a fraction of the source photons at each position. We account for the remaining flux when estimating count-rates and fluxes by applying a mean aperture correction determined by averaging the exposure-time weighted PSF corrections for individual sources.

5 RESULTS

5.1 X-ray properties of galaxies in the red cloud and in the transition zone

Table 1 summarises the fraction of X-ray detections among galaxy samples selected at several positions in the CMD. The X-ray identification rate is higher in the red cloud, in agreement with recent studies on the host galaxy properties of X-ray selected AGN (Nandra et al. 2007).

In this section, we search for evidence of obscured and/or low-luminosity systems below the X-ray detection threshold by stacking optically selected galaxies in different regions of the CMD. Of particular interest is the valley, where AGN are suggested to play an important role in galaxy evolution. The results for different subsamples are summarised in Table 2 and are plotted in Figure 3. There is some evidence for a progressive hardening of the stacked signal from the blue to the red cloud. This is further demonstrated in Figure 4 which plots the hardness ratio of galaxies in CMD slices which run parallel to the Willmer et al. (2006) line separating the blue from the red clouds. Although the errorbars of individual points are large, there is a systematic trend whereby the mean X-ray spectrum of 24 μm-bright sources becomes harder, reaching $\Gamma \approx 1.2$, for $\Delta C > -0.15$, i.e. for sources around the valley

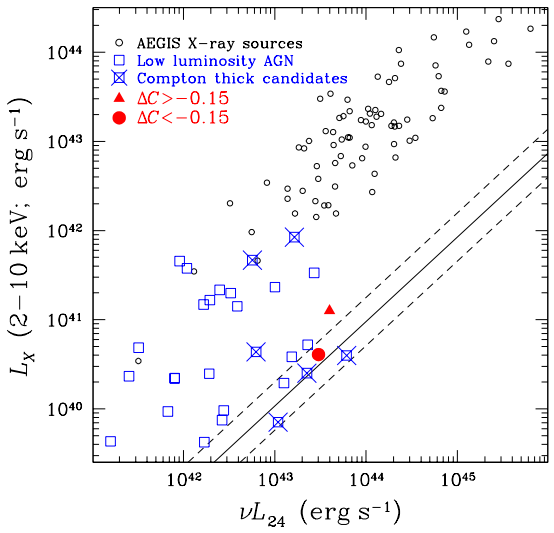

Figure 6. 2-10 keV X-ray luminosity against $24\,\mu$m luminosity. The continuous line is the $L_X - \nu L_{24}$ relation for star-forming galaxies adapted from Ranalli et al. (2003). The dashed lines correspond to the 1 sigma rms envelope around this relation. The (red) triangle corresponds to the mean νL_{24} and L_X for $24\,\mu$m-bright galaxies with $\Delta C > -0.15$. Similarly, the (red) filled circle is for $24\,\mu$m-bright galaxies with optical colours bluer than $\Delta C < -0.15$. The uncertainties in the luminosities of these two populations are smaller than the size of the points and are not plotted for clarity. The open (black) circles are AEGIS X-ray AGN selected in the hard X-ray band (2-10 keV). Also shown is the local sample of low-luminosity AGN (open blue squares), which includes Compton thick candidates (crossed blue squares), from Terashima et al. (2002). The mid-IR luminosity of individual AEGIS X-ray sources, $\nu L_{24\mu m}$, is estimated from the $24\,\mu$m flux density by adopting the SED of NGC 1068 for the k-correction. The conclusions are not sensitive to this assumption. Also, for AEGIS X-ray sources the $L_X(2-10\,\mathrm{keV})$ is calculated from the 2-10 keV observed-frame flux using a typical intrinsic AGN spectrum of $\Gamma = 1.9$ (Nandra & Pounds 1994). This effectively produces absorption-corrected fluxes for sources with column densities $N_H < 10^{23}\,\mathrm{cm}^{-2}$ at $z \approx 1$. For the Terashima et al. (2002) low-luminosity AGN we use the obscuration corrected luminosity listed by these authors, except in the case of Compton thick candidates, identified by the equivalent width of the FeK line, adopting the criterion EW > 900 eV. The 24μm luminosity of the Terashima et al. (2002) sources is estimated using the IRAS $25\,\mu$m flux density. The mean 24μm luminosity for the subsamples used in the stacking is estimated by taking the average of the $\nu L_{24\mu m}$ of individual sources. The mean $L_X(2-10\,\mathrm{keV})$ is estimated using the X-ray flux determined by the stacking analysis and the mean redshift of the sources in each subsample.

and in the red cloud. Bluer galaxies have hardness ratio upper limits (3σ) consistent with softer mean X-ray spectra, $\Gamma > 1.4$. The corresponding upper limits for the $24\,\mu$m-faint subsample do not provide strong constraints, but also suggest relatively soft spectral properties. In any case, there is no evidence that the mean hardness ratio of this population increases with ΔC at the same level as for $24\,\mu$m-bright galaxies.

In order to improve the statistics we split the $24\,\mu$m-bright sample at $\Delta C = -0.15$ and stacked separately sources bluer/redder than this limit. The resulting mean hardness ratio is plotted as a function of redshift in Figure 5. The mean hardness ratio of the $24\,\mu$m-bright population with $\Delta C > -0.15$ is harder than the ARP 220 starburst template and in better agreement with the obscured AGN models. In contrast, the hardness ratio of galaxies bluer than $\Delta C < -0.15$ is consistent with star-formation (i.e. X-ray binaries and hot gas), although we cannot exclude the possibility of low-luminosity unobscured AGN.

The obscured AGN interpretation for the $24\,\mu m$-bright population with $\Delta C > -0.15$ is also supported by Figure 6, which plots the 2-10 keV X-ray luminosity against the $24\,\mu$m luminosity, in comparison with the relation between these two quantities for star-forming galaxies adapted from Ranalli et al. (2003). Sources with $\Delta C > -0.15$ in this figure are X-ray luminous compared to this relation, suggesting that their stacked X-ray signal is dominated by AGN. The same conclusion applies if galaxies are split into finer colour bins, e.g. upper blue cloud ($-0.15 < \Delta C < -0.05$), valley ($-0.05 < \Delta C < -0.05$) and red cloud ($\Delta C > +0.05$). These subsamples have mean X-ray and $24\,\mu m$ luminosities similar to the overall $\Delta C > -0.15$ population and therefore are also X-ray luminous compared to the expectation from star-formation. These results are in contrast to the mean X-ray luminosity of $24\,\mu m$-bright galaxies with $\Delta C < -0.15$, which is consistent with the star-formation relation. These suggests that X-ray binaries and hot gas dominate the X-ray emission of this population.

5.2 X-ray properties of post-starbursts

An interesting trend in Table 1 is the higher fraction of X-ray sources in post-starbursts. In the red cloud in particular, where the majority of post-starbursts are found, 15 per cent of these systems are associated with X-ray sources. In contrast the X-ray identification rate is only 2 per cent for the overall optical galaxy population and about 4 per cent for galaxies in the red cloud. In order to assess the significance of the excess, we resampled the optical galaxy population to construct subsamples with size equal to the number of red-cloud post-starbursts and with similar M_B and $U-B$ distributions. The fraction of X-ray identifications in each subsample is registered and the experiment was repeated 10 000 times. The X-ray detection rate of the random subsamples is lower than that of post-starbursts in 98 per cent of the experiments. The excess of X-ray sources in this population is therefore significant at the 98 per cent level. Post-starbursts are also a non-negligible component of the X-ray population. In the redshift interval $0.68 \lesssim z \lesssim 0.88$, $21 \pm 10\%$ (5/24) of the X-ray sources in the red cloud have post-starburst optical spectra. For comparison the fraction of red cloud galaxies that are post-starbursts is 7 per cent (34/490). These results, although limited by small number statistics, tentatively suggest a link between AGN and the post-starburst stage of galaxy evolution at $z \approx 0.8$. The link is also supported by the mean stacked X-ray properties of post-starbursts not individually detected to the limit of AEGIS *Chandra* survey. The post-starburst population is marginally detected in both the soft and the hard spectral bands at a significance level $\gtrsim 3\sigma$ (Table 2, column 7). Although the stacked signal is not dominated by a single source just below the X-ray detection threshold, small number statistics are a concern. The results in Table 2, taken at face value, are consistent with $\Gamma \approx 0.7$. This is much harder than the X-ray spectrum of star-forming galaxies (Figure 5) or unobscured AGN ($\Gamma \approx 1.9$; Nandra & Pounds 1994) suggesting that absorption is suppressing the soft X-ray emission from the central engine in these systems.

5.3 Optical morphology: interactions and star-formation

In the previous sections, we found evidence for AGN activity among $24\,\mu$m-bright galaxies with $\Delta C > -0.15$ (which includes post-starbursts). This cut includes the reddest part of the

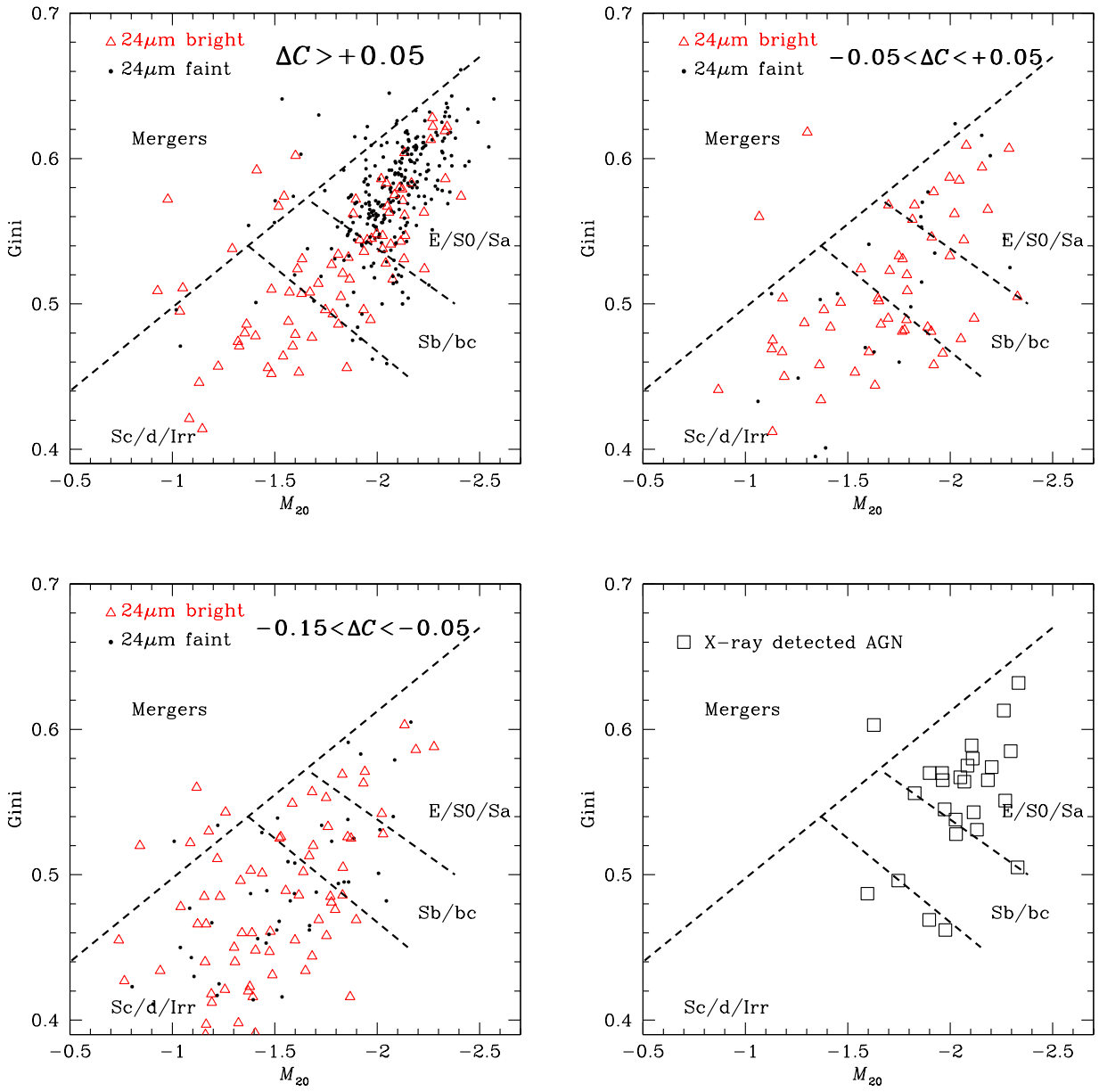

Figure 7. Gini against M_{20} diagrams. The regions of the parameter space occupied by different galaxy types are demarcated with the dashed lines. For clarity sources at different parts of the CMD are plotted in different panels: upper left sources with $\Delta C > +0.05$, upper right $-0.05 < \Delta C < +0.05$ (valley), lower left $-0.15 < \Delta C < -0.05$ (upper blue cloud). In all these panels open triangles are 24μm bright sources and the dots are for 24μm faint galaxies. In the lower right panel we show the position of X-ray detected AGN on the Gini–M_{20} diagram.

blue cloud, the valley, and the red cloud. The optical morphology of these sources should be a powerful diagnostic of their nature. Are they interacting/merging systems? Do they show evidence for star-formation? For classifying galaxies into different morphological types, we use the *HST*/ACS data to estimate the Gini coefficient, which measures the clumpiness of a source, and the second moment of the brightest 20% pixels of the galaxy, M_{20} (Lotz, Primack & Madau 2004), which measures the central concentration of a galaxy. Different Hubble types are separated in the Gini–M_{20} diagram and the morphological classification based on these two non-parametric estimators remains robust at high redshift. An additional parameter, the asymmetry, is also used to search for disturbances that might indicate recent/ongoing interactions (e.g. Abraham et al. 1996; Conselice et al. 2000). This parameter measures the degree to which the light of the galaxy is rotationally symmetric.

Figure 7 plots the Gini–M_{20} parameters for galaxies with $\Delta C > -0.15$. While the $24\,\mu m$-bright population with $\Delta C > -0.15$ includes systems classified as ongoing mergers, these are about 7 per cent of the population. The majority of the $24\,\mu m$-bright sources in Figure 7, about 70 per cent, have spiral or irregular morphology, Sb or later. Blue star-forming regions in these galaxies are indeed resolved by the *HST*. The $24\,\mu m$ emission of

Table 2. Stacking results

Sample	N	$< z >$	band	T	B	S/N (σ)	photon rate (10^{-9})	HR	f_X (10^{-17})	$\log L_X$ (erg/s)
(1)	(2)	(3)	(4)	(5)	(6)	(7)	(8)	(9)	(10)	
red cloud ($\Delta C > 0.0$)										
all	881	0.67	soft	741	389.9	17.9	9.6 ± 0.9	-0.16 ± 0.09	1.7 ± 0.2	40.4
			hard	1178	892.4	9.6	7.0 ± 1.1		6.4 ± 1.0	40.9
24μm-bright	177	0.69	soft	169	80.8	9.8	10.7 ± 1.9	0.01 ± 0.14	1.9 ± 0.3	40.4
			hard	286	187.5	7.2	10.8 ± 2.4		10.7 ± 2.4	41.2
24μm-faint	513	0.66	soft	451	235.2	14.1	9.5 ± 1.2	-0.27 ± 0.12	1.6 ± 0.2	40.4
			hard	676	537.3	6.0	5.5 ± 1.4		4.7 ± 1.2	40.8
valley ($-0.05 < \Delta C < +0.05$)										
all	188	0.68	soft	155	81.8	8.1	9.5 ± 2.0	-0.23 ± 0.21	1.6 ± 0.3	40.4
			hard	238	187.1	3.7	6.0 ± 2.4		5.3 ± 2.1	40.9
24μm-bright	89	0.70	soft	85	41.0	6.9	11.4 ± 2.9	-0.09 ± 0.22	2.0 ± 0.5	40.5
			hard	113	92.3	4.2	9.5 ± 3.5		9.0 ± 3.3	41.1
24μm-faint	61	0.68	soft	42	26.1	3.1	5.8 ± 3.0	<0.15	1.0 ± 0.5	40.3
			hard	61	60.7	0.0	<7.8		<6.9	<41.1
blue cloud ($\Delta C < 0.0$)										
all	3331	0.66	soft	2009	1469.1	14.1	3.9 ± 0.4	-0.52 ± 0.15	0.6 ± 0.1	40.0
			hard	3565	3375.7	3.3	1.2 ± 0.5		0.9 ± 0.4	40.2
24μm-bright	572	0.68	soft	538	269.0	15.8	9.7 ± 1.1	-0.37 ± 0.12	1.6 ± 0.2	40.4
			hard	745	613.6	5.3	4.4 ± 1.2		3.6 ± 1.0	40.8
24μm-faint	1811	0.66	soft	1018	823.7	6.8	2.4 ± 0.5	< -0.24	0.4 ± 0.1	39.8
			hard	1910	1897.2	0.3	<1.4		<1.2	<40.3
$\Delta C > -0.15$										
all	1270	0.67	soft	1017	560.5	19.3	8.7 ± 0.7	-0.17 ± 0.08	1.5 ± 0.1	40.3
			hard	1643	1279.8	10.2	6.2 ± 0.9		5.7 ± 0.8	40.9
24μm-bright	332	0.69	soft	300	153.6	11.8	9.5 ± 1.4	$+0.00 \pm 0.12$	1.7 ± 0.2	40.4
			hard	516	352.7	8.7	9.5 ± 1.7		9.4 ± 1.7	41.1
24μm-faint	648	0.66	soft	531	294.4	13.8	8.2 ± 1.0	-0.31 ± 0.13	1.4 ± 0.2	40.3
			hard	810	671	5.3	4.35 ± 1.2		3.7 ± 1.0	40.8
$\Delta C < -0.15$										
all	2942	0.66	soft	1733	1298.5	12.1	3.5 ± 0.5	< -0.49	0.6 ± 0.1	40.0
			hard	3100	2988.3	2.0	< 1.2		< 0.9	<40.2
24μm-bright	417	0.67	soft	397	196.2	14.3	10.3 ± 1.3	-0.54 ± 0.16	1.7 ± 0.2	40.5
			hard	515	448.4	3.2	3.1 ± 1.4		2.4 ± 1.1	40.6
24μm-faint	1676	0.66	soft	938	764.6	6.3	2.3 ± 0.5	< -0.21	0.4 ± 0.1	39.8
			hard	1776	1763	0.3	< 1.5		<1.2	<40.3
post-starburst	26	0.76	soft	20	13.7	1.7	<7.5	$> +0.35$	<1.4	<40.3
			hard	44	25.9	3.6	15.5 ± 7.1		17.8 ± 8.2	41.4

The columns are: (1): Sample definition. The redshift interval is $0.4 - 0.9$ for all samples except for post-starbursts; (2): number of sources used for stacking after excluding galaxies that lie close to or associated with X-ray detections; (3): mean redshift of the sample; (4): spectral band where X-ray photons are stacked: soft: 0.5–2 keV and hard: 2–7 keV; (5): Total counts (source+background) within the extraction radius; (6): Background counts; (7): significance of the detected signal estimated from the relation $(T - B)/\sqrt{B}$ and expressed in background standard deviations; (8): Photon count rate in units of $10^{-9}\,\mathrm{s}^{-1}$ corrected for aperture effects and the *Chandra* response. In the case of non-detection the 3σ upper limit is listed; (9): Hardness ratio defined as (H-S)/(H+S) where H, S are the hard and soft band photon count rates respectively. The errors are estimated assuming Poisson statistics; (10): Rest-frame X-ray flux in units of $10^{-17}\,\mathrm{erg\,s^{-1}\,cm^{-2}}$ estimated in the 0.5-2 and 2-10 keV spectral bands adopting the mean power-law spectral index consistent with the HR. In the case of non-detection the 3σ upper limit is listed; (11): Logarithm of rest-frame luminosity in units of $\mathrm{erg\,s^{-1}}$.

these systems is also likely associated with young stars. Moreover, visual inspection of the *HST*/ACS images further shows that many $24\,\mu m$-bright sources in the E/S0/Sa region of the Gini-M_{20} diagram also have disks in addition to the dominant bulge, i.e. early type spirals. Similarly, visual inspection of the HST/ACS images of the X-ray detected AGN, also plotted in Figure 7, suggests that about half of these systems are associated with spirals. The morphological evidence above suggests that disks represent a substantial fraction of the $24\,\mu m$-bright galaxies with $\Delta C > -0.15$ and about half of the X-ray detected AGN. This suggests that (i) some level of star-formation is likely taking place in the host galaxy and (ii) recent major mergers are unlikely to have played a central role in the evolution of these sources.

Although major mergers do not appear to be frequent among

$24\,\mu m$-bright galaxies with $\Delta C > -0.15$ tidal disruptions, or minor mergers may play a role in their evolution. Figure 8 compares the distribution of the asymmetry parameter for the $24\,\mu$m-bright and the $24\,\mu$m-faint galaxies in the $\Delta C > -0.15$ part of the CMD. The panels in this figure correspond to different Hubble types based on the Gini-M_{20} classification of Figure 7. In the E/S0/Sa and Sb/bc panels, the $24\,\mu$m-bright sample is offset to higher asymmetries compared to the $24\,\mu$m-faint galaxies. For later Hubble types, Sc/d/Irr, there is little difference between the two subsamples. A Kolmogorov-Smirnov tests shows that the likelihood of the observed differences if the $24\,\mu m$-bright and $24\,\mu$m-faint samples were drawn from the same parent population is $< 10^{-6}$, 7×10^{-6}, and 0.15 for the E/S0/Sa, Sb/bc and Sc/d/Irr classes, respectively. For comparison, X-ray detected AGN, most of which are in the E/S0/Sa part of the Gini-M_{20} diagram, are also offset to higher asymmetries compared to early-type $24\,\mu$m-faint galaxies. This evidence suggests that minor gravitational encounters play a role in the evolution of both the $24\,\mu$m-bright systems with early-type optical morphology (E/S0/Sa and Sb/bc) and some of X-ray detected AGN associated with disks. Alternatively clumpy star-formation in the disk of galaxies can also produce the same effect, i.e. higher asymmetry parameter distribution. Differentiating between the two interpretations is not easy, and it is likely that clumpy star-formation and minor galaxy interactions are linked (e.g. Bell et al. 2005).

For late type galaxies (Sc/d/Irr) there is no statistically significant difference in the asymmetry parameter distribution between $24\,\mu$m-bright/faint sources. The two populations however, have distinct M_B distributions, suggesting differences in their stellar mass. This is shown in Figure 9, where late-type $24\,\mu m$-bright galaxies with $\Delta C > -0.15$ have mean absolute B-band magnitude $M_B \approx -20.8$ mag. This is more luminous than the average $M_B \approx -20.0$ mag for $24\,\mu m$-faint sources of similar morphological type. The two populations also have similar rest-frame colour distributions suggesting similar mass–to–light ratios, M/L. Adopting $\log \mathrm{M/L} = +0.1$, consistent with the colours of the galaxies in the sample (Bell & de Jong 2001), the above mean optical luminosities translate to stellar masses of $\approx 4 \times 10^{10}$ and $2 \times 10^{10}\,\mathrm{M}_\odot$ for $24\,\mu$m-bright and faint sources respectively.

A plausible interpretation of the results above is that AGN activity requires a massive BH and some gas to fuel it (Kauffmann et al. 2003). Massive galaxies often host large BHs, while star-formation is an indication of gas availability. The $24\,\mu m$-bright galaxies with $\Delta C > -0.15$ are typically luminous, $M_B \lesssim -20$ mag, and therefore most likely massive. The morphological evidence above also indicates star-formation in a large fraction of these systems. This is contrary to $24\,\mu m$-faint galaxies, which are either quiescent and/or less massive than $24\,\mu m$-bright sources. Galaxy encounters, not necessarily major mergers, may still be required in the picture above to disturb the gas to the galaxy centre and also to trigger the formation of stars.

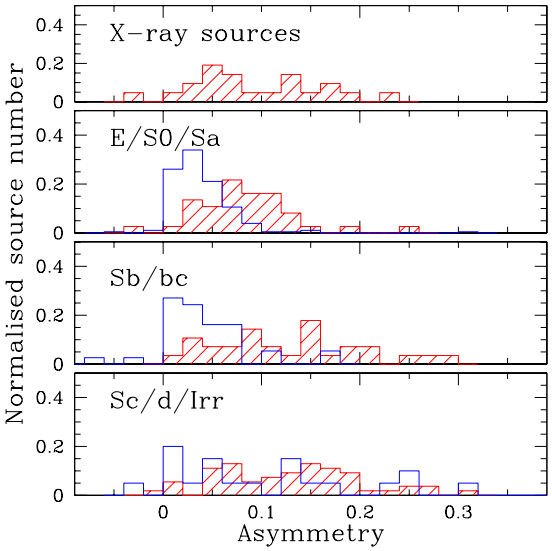

Figure 8. Normalised distribution of the asymmetry parameter for $24\,\mu$m-bright (hatched red histogram) and 24μm-faint galaxies (open blue histogram) with $\Delta C > -0.15$. The different panels correspond to different morphological types defined using the Gini-M_{20} diagram shown in Figure 7. X-ray detected AGN in the AEGIS are plotted in the top panel.

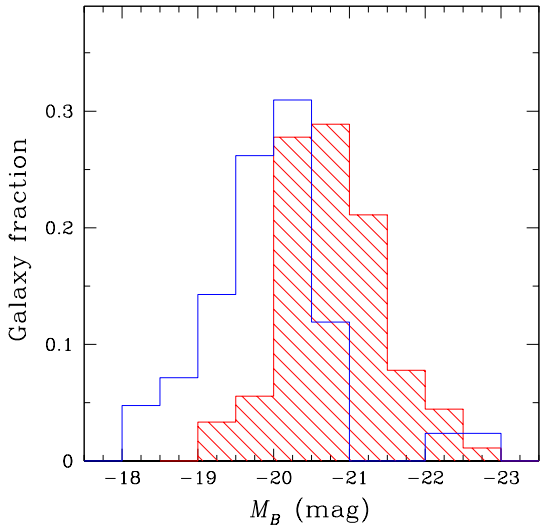

Figure 9. Normalised distribution of the absolute B-band magnitude for $24\,\mu$m-bright (hatched red histogram) and 24μm faint galaxies (open blue histogram) with late-type optical morphology (Sc/d/Irr) and $\Delta C > -0.15$.

5.4 The nature of AGN activity in transition zone and red galaxies

The X-ray hardness ratio $\gtrsim -0.1$ estimated in sections 5.1 and 5.2 for $24\,\mu$m-bright galaxies with $\Delta C > -0.15$ and post-starbursts can be attributed to low-luminosity Compton thin AGN, Compton thick sources (e.g. Figure 5), or radiatively inefficient accretion flows (e.g. Brand et al. 2005). Figure 6 shows that the average $24\,\mu$m-bright but X-ray undetected galaxy with $\Delta C > -0.15$ has X-ray luminosity about a factor 10 below the typical X-ray detected AGN. The X-ray undetected galaxies lie in the same region of the parameter space with moderately obscured low-luminosity AGN and Compton thick sources, suggesting that the observed stacked signal may be associated with one or the other type of AGN activity, or possibly with a mix of both. If the mid-IR luminosity of $24\,\mu m$-bright galaxies with $\Delta C > -0.15$ is, on average, dominated by star-formation, and not by dust heated by the central engine, then the moderately obscured low luminosity AGN scenario is most probable. We note however, that star-formation in the host

galaxy is also likely to contribute or even dominate the mid-IR emission of both the Terashima et al. comparison sample and the X-ray sources in the AEGIS survey. In the case of Compton thick activity, the intrinsic AGN luminosity is expected to be 100–1000 times brighter than the observed one (e.g. Iwasawa et al. 1997). Deeply buried AGN with luminosities approaching those of QSOs ($L_X \approx 10^{44}\,\mathrm{erg\,s^{-1}}$) among the red galaxies in this study cannot be ruled. Such objects are postulated to match the spectrum of the diffuse X-ray background (e.g. Gilli et al. 2007), but, currently, few have been securely identified (e.g. Georgantopoulos & Georgakakis 2007; Tozzi et al. 2006). Selection methods that include mid-IR wavelengths, like the one used here ($24\mu m$-bright and $\Delta C > -0.15$) , are capable of detecting this population (e.g. Lacy et al. 2004; Stern et al. 2005; Martinez-Sansigre et al. 2006; Donley et al. 2007). X-ray stacking analysis has indeed confirmed that at least some of these methods produce samples with hard mean X-ray spectra that are consistent with heavily obscured AGN (e.g. Daddi et al. 2007; Fiore et al. 2007; Georgantopoulos et al. 2007).

Brand et al. (2005) also reported a hard stacked X-ray signal for red galaxies in the range $0.3 < z < 0.9$ selected in the XBootes field of the NOAO Deep Wide-Field Survey (Kenter et al. 2005). These authors suggested that the detected signal can be interpreted as unabsorbed emission from a radiatively inefficient accretion (such as ADAFs; Narayan & Yi 1994, 1995). We explore this possibility by comparing the mean Eddington ratio of $24\mu m$-bright galaxies with $\Delta C > -0.15$ with that of M 87, the best studied example of a system undergoing radiatively inefficient accretion. The central supermassive BH of this galaxy has been shown to have very low radiative efficiency, corresponding to an Eddington ratio of $\approx 10^{-7}$ (Di Matteo et al. 2003). The mean optical absolute magnitude of $24\mu m$-bright galaxies with $\Delta C > -0.15$ is $M_B \approx -20.8$ mag, which corresponds to a mean stellar mass of $4 \times 10^{10}\,\mathrm{M_\odot}$ for a mass–to–light ratio of $\log \mathrm{M/L} = +0.1$, consistent with the average colours of the galaxies with $\Delta C > -0.15$ (Bell & de Jong 2001). Assuming that the bulk of the stellar mass is associated with the galaxy bulge and using the relation between BH mass and bulge dynamical mass of Häring & Rix (2004), we estimate a BH mass of $6 \times 10^7\,\mathrm{M_\odot}$. This is an upper limit as the estimated stellar mass of the $24\mu m$-bright population may have a large contribution from the disk of these galaxies, which has been ignored in this exercise. The mean 2-10 keV X-ray luminosity of this population (Table 2) corresponds to a bolometric luminosity of $L_{bol} = 3.5 \times 10^{42}\,\mathrm{erg\,s^{-1}}$, adopting the bolometric correction of Elvis et al. (1994). This is a lower limit in the case of Compton thick activity. The BH mass and the L_{bol} estimates above translate to a *lower* limit for the Eddington ratio of $\approx 5 \times 10^{-4}$, more than 3 dex higher than the corresponding quantity for M 87. If the hard X-ray signal of $24\mu m$-bright galaxies with $\Delta C > -0.15$ is associated with a radiatively inefficient accretion mode, they have to be significantly less extreme than M 87. For comparison, X-ray *detected* AGN at $z \approx 1$ have Eddington ratios in the range $10^{-4} - 10^{-1}$ (e.g. Bundy et al. 2007; Babic et al. 2007). The mean Eddington ratio of the $24\mu m$-bright galaxies with $\Delta C > -0.15$ lies at the low-end of the interval above, suggesting that they are dominated by low luminosity and/or Compton Thick AGN.

6 DISCUSSION

6.1 AGN and transition zone galaxies

In the nearby Universe, $z \lesssim 0.1$ there has been evidence for an association between *optically* selected AGN, recent star-formation and galaxies in the transition zone from the blue to the red cloud. Kauffmann et al. (2003) found that luminous AGN in the SDSS are hosted by early-type bulge-dominated galaxies that have stopped forming stars, but only in the *recent* past. Martin et al. (2007) extended this study by constructing the near-UV/optical CMD of galaxies at $z < 0.1$ using data from the GALEX Medium Imaging Survey and the SDSS. The density of Seyfert-2s in that sample, identified by diagnostic emission line ratios, peaks in the valley between the two clouds. Our work extends these results to higher redshift, $z \approx 0.7$, by finding evidence for obscured AGN among galaxies in the vicinity of the valley of the CMD and in the red cloud. Similar results also apply to the X-ray *detected* AGN population. X-ray sources with $\Delta C > -0.15$ have an average hardness ratio of -0.09 ± 0.07, while for those with $\Delta C < -0.15$ the mean hardness ratio is -0.31 ± 0.08.

The incidence of AGN among transition zone galaxies suggests that BH accretion may play a role in the evolution of these systems. This link has been highlighted recently by Hopkins et al. (2007) who show that the buildup rate of the red cloud mass function is in good agreement with predictions based on the QSO luminosity function. This calculation assumes either a fixed Eddington accretion rate for QSOs and the local BH-host mass empirical relation or a more physically motivated model for the QSO evolution based on simulations where BH accretion is triggered by gas-rich galaxy mergers (Hopkins et al. 2006a, b). Hopkins et al. (2007) also found that the observed rate of galaxy mergers and their distribution in stellar mass at different redshifts are broadly consistent with the growth rate of the red cloud mass function. The evidence above suggests an association between AGN activity, the transition of galaxies to the red cloud, and mergers. These catastrophic events can lead to the morphological transformation of galaxies and at the same time offer an efficient way for channeling gas to the nuclear regions of the galaxy, triggering the growth of the central BH.

Although our analysis broadly supports an association between AGN and galaxies on the move to the red cloud, the evidence for a causal link between the two is less clear. The X-ray spectra of AGN in the red cloud (both detections and stacking results) imply at least moderate amounts of obscuration in a large fraction of these systems. This is counter-intuitive to a picture where AGN-driven outflows blow away the gas and dust clouds from the nuclear galaxy regions and suggests that some gas and dust clouds either remain at or relax to the centre of the galaxy after the quenching of the star-formation to form a torus. Additionally, major mergers are not supported by the data. Minor mergers or tidal disruptions may still play a role in the evolution of $24\mu m$-bright galaxies with $\Delta C > -0.15$. Recent studies on the evolution of the star-formation since $z \approx 1$ also suggest that a decline in the major mergers is not the dominant physical mechanism driving the evolution. Gas exhaustion in disk galaxies that form stars in a quiescent mode may be more important (e.g. Bell et al. 2005; Wolf et al. 2005; Melbourne, Koo & Le Floch 2005; Noeske et al. 2007a, b). The gas depletion scenario is also consistent with the obscured AGN activity observed in galaxies in the transition zone and in the red cloud.

6.2 AGN in post-starbursts

In the local Universe, $z < 0.1$, an increasing body of evidence points to a link between black-hole accretion and post-starbursts. Yan et al. (2006) performed a systematic search for post-starbursts in the SDSS using methods similar to those described here. A large fraction of the sources in that sample (> 70 per cent) show weak emission lines consistent with low-luminosity and/or obscured AGN, e.g. LINERs, Seyfert-2s, transition objects. In a complementary study Goto (2006) selected SDSS galaxies with deep Hδ absorption and emission line signatures typical of AGN. These sources represent about 4 per cent of the AGN in a volume limited sample, much higher than in the overall SDSS population (0.2 per cent).

Our results extend the association between AGN and postastabursts to high redshift, $z \approx 0.8$. Firstly, there is an increased fraction of X-ray detected AGN among the post-starburst galaxy population. Secondly, about 20 per cent of the red-cloud AGN in the redshift interval $0.7 \lesssim z \lesssim 0.9$, where post-starbursts can be identified, are hosted by such galaxies. Most of the X-ray detected post-starbursts are obscured, with an average hardness ratio of ≈ -0.09. Thirdly, stacking the X-ray photons at the positions of post-starbursts that are not individually detected at X-ray wavelengths, reveals a hard mean X-ray spectrum and suggests obscured AGN activity in the bulk of this population.

The low redshift, post-starburst sample of Yan et al. (2006) is comparable in terms of selection to that presented here. Most of the emission line sources in that sample belong to the LINER class. These low-luminosity AGN often show hard X-ray spectra and, in many cases, are associated with moderate column densities, $\mathrm{N_H} \approx 10^{22} - 10^{23}\,\mathrm{cm}^{-2}$, or even Compton thick systems where the X-ray emission is dominated by reflected radiation (e.g. Terashima et al. 2002; González-Martín et al. 2006). In the latter case, the intrinsic AGN power is likely to be significantly higher than the observed one. The evidence above suggests a similar nature for the $z \approx 0.8$ post-starbursts for which our analysis shows a hard X-ray spectrum in the mean. While the incidence of AGN in post-starbursts is consistent with models where BH accretion is responsible for quenching the star-formation in galaxies, the fact than many of these AGN are obscured means that gas and dust clouds remain in the nuclear galaxy regions, possibly in a form of a torus, after the AGN-driven blow-out phase.

6.3 Obscured AGN in the red cloud

A striking result from this study is that the red cloud includes a large population of obscured AGN, both above and below the X-ray detection threshold of the AEGIS *Chandra* survey. This extends recent studies, which have shown that a large fraction of the X-ray *detected* AGN at $z \approx 1$, and certainly, the majority of the obscured ones, are hosted by red galaxies (e.g. Georgakakis, Georgantopoulos & Akylas 2006; Nandra et al. 2007; Rovilos & Georgantopoulos 2007).

The incidence of a large population of obscured AGN in the red cloud suggests that the BH accretion outlives the termination of star-formation. This is also supported by the X-ray properties of post-starburst galaxies in our study. It is not clear why such a large fraction of red cloud galaxies and post-starbursts show high column densities. If these sources represent systems after the AGN driven termination of star-formation then one would expect the central engine to be unobscured. The X-ray obscuration in these systems may therefore represent cold gas that either has not been blown out, or has not been processed and which relaxes to the galaxy centre to form a torus surrounding the central engine (e.g. Hopkins et al. 2006a). Alternatively, gas exhaustion and not necessarily outflows driven by accreting BHs, may be the mechanism behind the evolution of both AGN and galaxies. In this picture the AGN may remain obscured as long as there are dust and gas clouds to feed the central BH. Also, some of the red cloud $24\mu\mathrm{m}$ bright sources may be dusty systems (hence the red colour) observed before the quenching of the star-formation.

The large fraction of obscured AGN in the red cloud is contrary to the distribution of *optically* selected, low redshift AGN in the GALEX near-UV/optical CMD (Martin et al. 2007). The number density of Seyfert-2s in that study peaks in the valley. This discrepancy may be related to selection effects. For example, dilution of the emission lines by the host galaxy stellar population makes the identification of the AGN optical spectral signatures difficult (e.g. Comastri et al. 2002; Severgnini et al. 2003; Georgantopoulos & Georgakakis 2005). Also, contamination of the GALEX near-UV band by scattered AGN light will move red galaxies into the valley. Alternatively, the GALEX near-UV bands may be more sensitive to low level star-formation compared to optical wavebands. In any case, this potential discrepancy highlights the need to study in more detail the overlap and the differences between optical and X-ray AGN selection methods in terms of host galaxy properties.

7 CONCLUSIONS

We explore the role of AGN in establishing the bimodal colour distribution of galaxies by quenching the star-formation of blue star-forming systems causing their transformation to red, evolved galaxies. The main conclusions from this study are summarised below

1. There is evidence for AGN activity among galaxies in the transition zone between the red and blue clouds of the CMD. A large fraction of these accreting BHs are obscured, suggesting that if AGN outflows are related to the colour transformation of galaxies, at least some nuclear gas and dust gas clouds are either not affected or can efficiently reform after the truncation of the star-formation.

2. Morphological analysis suggests that major mergers do not dominate the evolution of this population. Minor interactions however, may play a role.

3. We find an association between BH accretion and post-starbursts at $z \approx 0.8$, in agreement with studies on the properties of AGN hosts at low redshift, $z \approx 0.1$.

4. AGN activity outlives the termination of the star-formation. A large fraction of active BHs are present in red cloud galaxies. This is in contrast to optically selected AGN, which lie predominantly in the valley between the two clouds.

8 ACKNOWLEDGEMENTS

We thank the referee, Rachel Somerville, for providing constructive comments and suggestions that significantly improved this paper. This work has been supported by funding from the Marie-Curie Fellowship grant MEIF-CT-2005-025108 (AG), STFC (ESL) and Chandra grant GO5-6141A (DCK). JML acknowledges support from the NOAO Leo Goldberg Fellowship, the NASA grants HST-GO-10314.13-A and HST-AR-10675-01-A from the Space Telescope Science Institute, which is operated by the AURA, Inc., under NASA contract NAS5-26555, NASA grant NAG5-11513 to P.

Madau. JAN is supported by NASA through Hubble Fellowship grant HF-011065.01-A, awarded by the Space Telescope Science Institute, which is operated by the Association of Universities for Research in Astronomy, Inc., for NASA, under contract NAS 5-26555.

Support for GO program 10134 was provided by NASA through NASA grant HST-G0-10134.18-A from the Space Telescope Science Institute, which is operated by the Association of Universities for Research in Astronomy, Inc., under NASA contract NAS 5-26555.

The authors wish to recognise and acknowledge the very significant cultural role and reverence that the summit of Mauna Kea has always had within the indigenous Hawaiian community. We are most fortunate to have the opportunity to conduct observations from this mountain. This work is based in part on observations made with the *Spitzer* Space Telescope, which is operated by the Jet Propulsion Laboratory, California Institute of Technology under a contract with NASA. Support for this work was provided by NASA through an award issued by JPL/Caltech.

REFERENCES

Abraham R. G., et al., 1996, ApJS, 107, 1
Alexander D. M., et al., 2005, Nature, 434, 738
Alexander D. M., et al., 2003, AJ, 126, 539
Babic A., Miller L., Jarvis M. J., Turner T. J., Alexander D. M., Croom S. M., 2007, A&A, 474, 755
Baldry I. K., Glazebrook K., Brinkmann J., Ivezic Z., Lupton R. H., Nichol R. C., Szalay A. S., 2004, ApJ, 600, 681
Barger A. J., et al., 2005, AJ, 129, 578
Barmby P., et al., 2006, ApJ, 642, 126
Bell E., Phleps S., Somerville R. S., Wolf C., Borch A., Meisenheimer K., 2006a, ApJ, 652, 270
Bell E., et al., 2006b, ApJ, 640, 241
Bell E., et al., 2005, ApJ, 625, 23
Bell E., et al., 2004, ApJ, 608, 752
Blanton M. R., 2006, ApJ, 648, 268
Brand K., et al., ApJ, 2005, 626, 723
Brusa M., et al., 2007, ApJS, 172, 353
Bundy K., et al., 2007, ApJ, submitted, arXiv0710.2105
Cattaneo A., et al., 2007, MNRAS, 377, 63
Cid Fernandes R., et al., 2001, ApJ, 558, 81
Conselice C. J., Bershady M. A., Jangren A., 2000, ApJ, 529, 886
Comastri A., et al., 2002, ApJ, 571, 771
Croton D. J, et al., 2006, MNRAS, 365, 11
Daddi E., et al., 2007, ApJ, submitted, arXiv:0705.2832
Dale D. A., et al., 2007, ApJ, 655, 863
Davis M., et al., 2007, ApJ, 660, 1L
Dekel A., Birnboim Y., 2006, MNRAS, 368, 2
Di Matteo T., Allen S. W., Fabia A. C. Fabian, Wilson A. S., Young A. J., ApJ, 2003, 582, 133.
Donley J. L., et al., 2005, ApJ, 634, 169
Elvis M., 1994, ApJS, 95, 1
Faber et al. 2003, SPIE, 4841, 1657
Fabian A. C., 1999, MNRAS, 308L, 39
Ferrarese L. & Merritt D., 2000, ApJ, 539, L9
Franceschini A., et al., 2003, MNRAS, 343, 1181
Fiore F., et al., 2007, ApJ, submitted, arXiv:0705.2864
Gebhardt K., et al., 2000, ApJ, 539, L13
Genzel R., et al., 1998, ApJ, 498, 579
Georgakakis A., Georgantopoulos I. & Akylas A., 2006, MNRAS, 366 ,171
Georgakakis A., Hopkins A. M., Afonso J., Sullivan M., Mobasher B., Cram L. E., 2004, MNRAS, 354, 127
Georgantopoulos I., et al., 2007, MNRAS, submitted
Georgantopoulos I. & Georgakakis A., 2007, A&A, 466, 823
Georgantopoulos I. & Georgakakis A., 2005, MNRAS, 358, 131
Gerke B. F., et al., 2007, MNRAS, 376, 1425
Gilli R., Comastri A., Hasinger G., 2007, A&A, 463, 79
González-Martín O., Masegosa J., Márquez I., Guerrero M. A., Dultzin-Hacyan D., 2006, A&A, 460, 45
Goto T., 2006, MNRAS, 369, 1765
Grogin N. A., 2005, ApJ, 627, 97L
Grogin N. A., et al., 2003, ApJ, 595, 685
Häring N. & Rix H. W., 2004, ApJ, 604L, 89
Hasinger G., Miyaji T., Schmidt M., 2005, A&A, 441, 417
Hopkins P. F., et al., 2005, ApJ, 630, 705
Hopkins P. F., Hernquist L., Cox T. J., Di Matteo T., Robertson B., S. Volker, 2006a, ApJS, 163, 1
Hopkins P. F., Somerville R. S., Hernquist L., Cox T. J., Robertson B., Li Y., 2006b, ApJ, 652, 864
Hopkins P. F., Bundy K., Hernquist L., Ellis R. S., 2007, ApJ, 659, 976
Iwasawa K., Fabian A. C., Matt G., 1997, MNRAS, 289, 443
Kauffmann G., et al., 2004, MNRAS, 353, 713
Kauffmann G., et al., 2003, MNRAS, 346, 1055
Kenter A., et al., 2005, ApJS, 161, 9
King A., 2003, ApJ, 596, 27L
Cirasuolo M., et al., 2007, MNRAS, submitted, arXiv:astro-ph/0609287
Lacy M., et al., 2004, ApJS, 154, 166
Laird E. S., Nandra K., Adelberger K. L., Steidel C. C., Reddy N. A., 2005, MNRAS, 359, 47
Lotz J. M., et al., 2007, ApJ, submitted, arXiv:astro-ph/0602088
Lotz J. M., Primack J., Madau P., 2004, AJ, 128, 163
Magorrian J., et al., 1998, AJ, 115, 2285
Martin C. D., et al., 2007, ApJS, in press, astro-ph: 0703281
Martinez-Sansigre A., et al., 2006, MNRAS, 370, 1479
Matt G., et al., 1999, A&A, 341, 39L
Melbourne J., Koo D. C., Le Floch E., 2005, ApJ, 632L, 65
Nandra K., et al., 2007, ApJ, 660, 11L
Nandra K., et al., 2005, MNRAS, 356, 568
Nandra K., Mushotzky R. F., Arnaud K., Steidel C. C., Adelberger K. L., Gardner J. P., Teplitz H. I., Windhorst R. A., 2002, ApJ, 576, 625
Nandra K. & Pounds K. A., 1994, MNRAS, 268, 405
Narayan R., Igumenshchev I. V., & Abramowicz M. A. 2000, ApJ, 539, 798
Narayan R., & Yi I., 1994, ApJ, 428, L13
Noeske K. G. et al., 2007a ,ApJ, 660L, 47
Noeske K. G. et al., 2007b ,ApJ, 660L, 43
Okamoto T., Nemmen R. S., Bower R. G., 2007, MNRAS, submitted, arXiv:0704.1218
Pierce C. M., et al., 2007, ApJ, 660, 19L
Ptak A., Heckman T., Levenson N. A., Weaver K., Strickland D., 2003, ApJ, 592, 782
Quintero A. D., et al. 2004, ApJ, 602, 190
Ranalli P., Comastri A., Setti G., 2003, A&A, 399, 39
Rovilos E., Georgakakis A., Georgantopoulos I., Afonso J., Koekemoer A. M., Mobasher B., Goudis C., 2007, A&A, 466, 119
Rovilos E. & Georgantopoulos I., 2007, A&A, 475, 115
Severgnini P., et al., 2003, A&A, 406, 483
Silk J., & Rees M. J. 1998, A&A, 331, 1L
Stern D., et al., 2005, ApJ, 631, 163
Strateva I., 2001, AJ, 122, 1861
Terashima Y., Iyomoto N., Ho L. C., Ptak A. F., 2002, ApJS, 139, 1
Tozzi P., et al., 2006, A&A, 451, 457
Weiner B. J., 2005, ApJ, 620, 595
Willmer C. N. A., et al., 2006, ApJ, 647, 853
Wolf C., et al., 2005, ApJ, 630, 771
Yan R. et al., 2006, ApJ, 648, 281
Yan L. et al., 2004, ApJS, 154, 60